

RSC Advances



This is an *Accepted Manuscript*, which has been through the Royal Society of Chemistry peer review process and has been accepted for publication.

Accepted Manuscripts are published online shortly after acceptance, before technical editing, formatting and proof reading. Using this free service, authors can make their results available to the community, in citable form, before we publish the edited article. This *Accepted Manuscript* will be replaced by the edited, formatted and paginated article as soon as this is available.

You can find more information about *Accepted Manuscripts* in the [Information for Authors](#).

Please note that technical editing may introduce minor changes to the text and/or graphics, which may alter content. The journal's standard [Terms & Conditions](#) and the [Ethical guidelines](#) still apply. In no event shall the Royal Society of Chemistry be held responsible for any errors or omissions in this *Accepted Manuscript* or any consequences arising from the use of any information it contains.

Improved hydrogen storage properties of MgH₂ by addition of Co₂NiO nanoparticles

N. Juahir¹, N. S. Mustafa¹, A. M. Sinin², M. Ismail^{1,*}

¹School of Ocean Engineering, Universiti Malaysia Terengganu, 21030 Kuala Terengganu,
Malaysia

²Centre for Foundation and Liberal Education, Universiti Malaysia Terengganu, 21030 Kuala
Terengganu, Malaysia

*Corresponding author. Tel: +609-6683487; Fax: +609-6683991

E-mail address: mohammadismail@umt.edu.my

Abstract

A sample of MgH_2 and 10 wt.% Co_2NiO was prepared by the ball milling technique. The hydrogen storage properties and reaction mechanism of the sample were examined. The temperature-programmed desorption result shows that the addition of 10 wt.% Co_2NiO to MgH_2 exhibited a lower onset desorption temperature of 300 °C, which was decreased to 117 and 70 °C compared to as-received and as-milled MgH_2 , respectively. The de/rehydrogenation kinetics of $\text{MgH}_2 + 10 \text{ wt.}\% \text{Co}_2\text{NiO}$ showed improvement compared to un-doped MgH_2 . The results of the Kissinger plot shows that the activation energy for the hydrogen desorption of MgH_2 was reduced to about 65.0 and 15.0 kJ/mol compared to as-received and as-milled MgH_2 , respectively. Meanwhile, the X-ray diffraction analysis shows the formation of a new phase of Mg-Co alloy and $\text{Co}_{1.29}\text{Ni}_{1.71}\text{O}_4$ after the dehydrogenation and rehydrogenation process. It is reasonable to conclude that the Co_2NiO additive plays a catalytic role through the formation of active species of Mg-Co alloy and $\text{Co}_{1.29}\text{Ni}_{1.71}\text{O}_4$ during the heating process, thus improving the hydrogen storage properties of MgH_2 .

1. Introduction

The U.S Department of Energy has established a minimum target of 5.5 wt.% ab/desorption hydrogen storage capacity for the year 2015.¹ MgH₂ can be seen as a promising material among metal hydrides due to its high gravimetric hydrogen storage (7.6wt.%), good reversibility, and low cost.² However, MgH₂ have deficiencies, including high decomposition temperature and slow desorption/absorption kinetics.³ In order to make MgH₂ feasible as one of the potential materials for solid state hydrogen storage, different approaches have been used including improving the surface and kinetics by ball milling,⁴ adding catalyst,^{5,6} and using the destabilization concept.⁷⁻¹² The addition of catalysts by ball milling into MgH₂ has produced a significant effect on hydrogen sorption properties,^{5,6} thus it has caught the interest of many researchers. Various additives have been doped into MgH₂ such as metal,¹³⁻¹⁵ alloy,^{16,17} metal oxide,¹⁸⁻²¹ metal halide,^{5,22-27} carbon materials,²⁸⁻³⁰ and metal hydrides.^{31,32}

The addition of transition metal oxides has shown promising results in the ab/desorption kinetics of MgH₂. This enhancement could be associated with a highly effective catalysis shown by the transition of metal compounds due to the high affinity of metal cation transition towards hydrogen.³³⁻³⁷ Besides that, transition metal oxides also can act as a good catalyst by facilitating the dissociation of hydrogen molecules and the recombination of hydrogen atom towards the molecular state.³⁸ It is believed that the additive oxide phase facilitates to overcome the MgO layer formed on the surface of MgH₂ particles, thus improving the reaction kinetics.^{39,40}

To the best of the author's knowledge, no reported study has used Co₂NiO nanoparticle as an additive for the hydrogen storage properties of MgH₂. The selection of Co₂NiO as an additive was driven from several studies, which used Ni- and Co-based additives. Ni- and Co-based additive have been given considerable attraction due to their ability to destabilize the

dehydrogenation of MgH_2 .^{41,42} Mao et al. reported that the dehydrogenation temperature and the sorption kinetics of MgH_2 were improved by doping with NiCl_2 or CoCl_2 . Their results suggest that all the dehydrogenation products MgCl_2 , Mg_2Ni and Mg_2Co may play an important role in improving the hydrogen sorption kinetic properties of MgH_2 , while MgCl_2 may play a dominant role.³⁸ A recent study by Cabo et al. showed that the addition of mesoporous Ni- and Co based oxides reduced the onset dehydrogenation temperature and lowered the activation energy of MgH_2 .⁴³ Meanwhile, Mandzhukova et al. reported that the addition of 10 wt.% nickel cobaltite, NiCo_2O_4 improved the dehydrogenation kinetics of MgH_2 .^{44,45}

In this paper, the additive effect of Co_2NiO nanoparticle on the hydrogen storage properties of MgH_2 was investigated. The aim of this study is to combine the *in situ* active species factors together thus enhancing the de/hydrogenation properties of MgH_2 . The hydrogen storage properties and reaction mechanism of MgH_2 and Co_2NiO were investigated using a Sieverts-type pressure-composition-temperature (PCT) apparatus, X-ray diffraction (XRD), differential scanning calorimetry (DSC), and scanning electron microscope (SEM).

2. Experimental details

MgH_2 (hydrogen storage grade, 98 % purity) and Co_2NiO (<150 nm size particle, 99 % trace material basis) were purchased from Alfa Aesar and Sigma Aldrich, respectively and were used as received without further purification. Sample handling was performed in an MBraun Unilab glove box filled with high-purity Ar atmosphere. Approximately 200 mg MgH_2 was added with 10 wt.% Co_2NiO . This mixture was loaded into a sealed stainless steel vial together with four hardened stainless balls. As-milled MgH_2 sample under the same condition was prepared for comparison. Ball milling was performed in a planetary ball mill (NQM-0.4) for 1h

by milling for 1/4 h, resting for 2 min, and then milling for another 1/4 h in a different direction for 3 cycles at the rate of 400 rpm. The ratio of the weight of the balls to the weight of the powder was 80:1.

The temperature-programmed desorption (TPD) and re/dehydrogenation kinetics experiments were performed in a Sieverts-type pressure-composition-temperature (PCT) apparatus (Advanced Materials Corporation). The sample was loaded into a sample vessel in the glove box. For the TPD experiment, the samples were heated in a vacuum chamber from room temperature to 450 °C with a heating rate of 5 °C/min and the lowest decomposition temperature determined by the amount of desorbed hydrogen. The re/dehydrogenation kinetics experiments were performed at temperature of 320 °C with hydrogen pressure of 30 atm and 1 atm, respectively.

The phase structure of as-milled samples, before and after desorption and after rehydrogenation were measured using Rigaku MiniFlex II Diffractometer with Cu K α radiation. Before the measurement, a small amount of sample was spread uniformly in the sample holder and wrapped with a plastic wrap to prevent oxidation. θ - 2θ scans were carried out over the diffraction angles from 20° to 80° at a speed of 2.00°/min. Meanwhile, the microstructure of the samples were characterized using a scanning electron microscope (SEM; JEOL JSM-6360LA) by preparing the samples on the surface of carbon tape and then coating it with gold spray under vacuumed condition. All samples were also prepared in the glove box in order to minimize oxidation. A DSC analysis was carried out using a Mettler Toledo TGA/DSC 1. About 5-6 mg weight of the sample was loaded in an alumina crucible in the glove box. The crucible was then placed in a sealed glass bottle in order to prevent oxidation during transportation from the glove

box to the DSC apparatus. The samples were heated from room temperature to 480-550 °C under Ar atmosphere with different heating rates. An empty alumina crucible was used for reference.

3. Results and discussion

The dehydrogenation behavior of as-received MgH₂, as-milled MgH₂, and the MgH₂ + 10 wt.% Co₂NiO composite was investigated using a Sieverts-type PCT apparatus. Fig.1 presents the temperature-programmed-desorption (TPD) performances of as-received MgH₂, as-milled MgH₂, and the MgH₂ doped with 10 wt.% Co₂NiO. From the TPD curves, it can be seen clearly that the addition of 10 wt.% of Co₂NiO decreased the onset decomposition temperature compared to as-milled and as-received MgH₂. The onset decomposition of as-received and as-milled MgH₂ was about 417 and 370 °C with a total dehydrogenation capacity of 6.2 and 5.4 wt.% H₂ at 450 °C, respectively. These results show that the ball milling process also has an influence in reducing the onset desorption temperature of MgH₂ due to the larger surface area in magnesium surfaces. Therefore, a higher diffusion hydrogen absorption can be achieved.^{4,19} However, the as-milled MgH₂ showed slightly lower hydrogen desorption capacity compared to as-received MgH₂, and this could happen due to the released hydrogen during ball milling process. MgH₂ + 10 wt.% Co₂NiO had a positive effect on the onset desorption temperature of MgH₂, since the desorption started at around 300 °C with a total dehydrogenation capacity of 5.3 wt.% hydrogen at 450 °C, which was lowered by 117 °C and 70 °C compared to the as-received and as-milled MgH₂. These results suggest that the Co₂NiO component in the doped MgH₂ could play a catalytic role and thus, improving the onset temperature of MgH₂.

Fig.2 shows the isothermal desorption kinetics curve for as-milled MgH₂ and MgH₂ + 10 wt.% Co₂NiO composite measured at 320 °C under 1.0 atm pressure. The result shows that the

sample doped with 10 wt.% Co_2NiO released about 2.5 wt.% hydrogen in 6 min. In contrast, almost no hydrogen was released in the same period by as-milled MgH_2 . Therefore, it can be assumed that Co_2NiO also had significant effect on improving the dehydrogenation kinetics of MgH_2 . Fig.3 shows the isothermal rehydrogenation kinetics for as-milled MgH_2 and $\text{MgH}_2 + 10$ wt.% Co_2NiO samples. The samples were soaked at a constant temperature of 320 °C and under 30.0 atm hydrogen pressure. The hydrogen absorbed by MgH_2 doped with 10 wt.% Co_2NiO samples reached about 2.5 wt.% hydrogen within 1.7 min, with a total hydrogen absorption of 3.75 wt.%. Meanwhile, as-milled MgH_2 took about 3.4 min to absorb the same amount of hydrogen with a total hydrogen absorption of 3.78 wt.%. It can be seen that the doped sample showed better rehydrogenation kinetics than as-milled MgH_2 . Taken together, these results suggest that the rehydrogenation kinetics of MgH_2 can also be improved by doping it with Co_2NiO .

Fig. 4 represents the cyclic performance of $\text{MgH}_2 + 10$ wt.% Co_2NiO sample at temperature of 320 °C and under 30 atm hydrogen pressure. The hydrogen absorption kinetics of the sample shows some degradation after prolonged cyclic. However, the degradation was involving small values. After the 10th cycle, the absorption continued to be good with hydrogen capacity of 3.44 wt.%. Meanwhile, the cycle performances for the desorption kinetics of $\text{MgH}_2 + 10$ wt.% Co_2NiO sample also shows good performances even after 10th cycle as shown in Fig. 5 with the desorption kinetics of the sample in 60 minutes for 10th cycle was 3.75 wt.%. The hydrogen desorption also degrades after prolonged time with involving small amount hydrogen. This result shows that the good cyclic performances of MgH_2 can be achieved by doping with Co_2NiO .

Fig. 6 shows the recyclability capacity of the $\text{MgH}_2 + 10 \text{ wt.}\% \text{Co}_2\text{NiO}$ sample after 60 min absorb/desorb for the ten cycles. From the graph, it can be seen that for all cycles, the hydrogen desorption have slightly higher capacity compared to hydrogen absorption. It can be seen that the amount of hydrogen absorbed and desorbed degrades after prolonged cyclic. For hydrogen desorption, shows only slight degradation observed in hydrogen capacity of the 5th to 10th cycles compared to amount degrades for the first four cycles.

Fig. 7 presents the DSC curves of the $\text{MgH}_2 + 10 \text{ wt.}\% \text{Co}_2\text{NiO}$ sample at a heating rate of $15 \text{ }^\circ\text{C}/\text{min}$. As-received MgH_2 and as-milled MgH_2 were included for comparison purposes. The DSC curve of as-received MgH_2 showed only one strong endothermic peak at approximately $454.06 \text{ }^\circ\text{C}$, which corresponds to the decomposition of MgH_2 . Meanwhile, the DSC curves for as-milled MgH_2 and $\text{MgH}_2 + 10 \text{ wt.}\% \text{Co}_2\text{NiO}$ had strong endothermic peaks at $418.72 \text{ }^\circ\text{C}$ and $412.66 \text{ }^\circ\text{C}$, respectively. The noticeable reduction in the peak temperatures of the samples based on the DSC results revealed that dehydrogenation was improved by adding Co_2NiO . However, it could be seen that the onset decomposition temperature of the samples in DSC were slightly higher than those in TPD (Fig. 1), which could be due to the differences in heating rates and atmospheres between DSC and PCT measurements, as discussed in our previous papers.⁴⁶⁻⁴⁹ TPD measurement was conducted from 1.0 atm vacuum with a $5 \text{ }^\circ\text{C}/\text{min}$ heating rate, while DSC measurement was run under 1.0 atm argon flow with heating rate of $15 \text{ }^\circ\text{C}/\text{min}$.

The Kissinger equation⁵⁰ was used to calculate the activation energy (E_A) of $\text{MgH}_2 + 10 \text{ wt.}\% \text{Co}_2\text{NiO}$ at different heating rates. The activation energy of as-received and as-milled MgH_2 was included for comparison purposes. Fig. 8 (a) – (c) shows the DSC curves at different heating rates for as-received MgH_2 , as-milled MgH_2 , and $\text{MgH}_2 + 10 \text{ wt.}\% \text{Co}_2\text{NiO}$, respectively. From the Kissinger equation:

$$\ln [\beta / T_p^2] = -E_A/RT_p + A \quad (1)$$

where β is the heating rate, T_p is the peak temperature in the DSC curve, R is the gas constant, and A is a linear constant. Thus, the activation energy, E_A , can be obtained from the slope of the plot, $\ln [\beta / T_p^2]$ versus $1000/T_p$. Fig.8 (d) shows the Kissinger plot for the dehydrogenation of $\text{MgH}_2 + 10 \text{ wt.}\% \text{ Co}_2\text{NiO}$ composite compared to as-received and as-milled MgH_2 . The apparent activation energy for $\text{MgH}_2 + 10 \text{ wt.}\% \text{ Co}_2\text{NiO}$ composite estimated from the Kissinger analysis was found to be 118.0 kJ/mol, which was lower than that of as-received and as-milled MgH_2 (183.0 and 133.0 kJ/mol, respectively). These values show that improved dehydrogenation behavior and reduced activation energy can be achieved by doping Co_2NiO with MgH_2 .

Fig. 9 (a)-(c) show the SEM images of as-received MgH_2 , as-milled MgH_2 , and $\text{MgH}_2 + 10 \text{ wt.}\% \text{ Co}_2\text{NiO}$, respectively. In Fig. 9 (a), it can be seen that as-received particles of MgH_2 were angular shaped with sizes larger than 100 μm . Fig. 9 (b) shows a sample subjected to 1 h ball milling process, which caused a drastic reduction in MgH_2 particles with non-homogenous particles size. Besides that, some agglomeration was detected in the sample. After introducing Co_2NiO through the ball milling process, the size of the particles became smaller compared to as-milled MgH_2 sample (Fig. 9 (c)). The hardness of the Co_2NiO helped in breaking MgH_2 particles into smaller sizes, increasing the specific surface area and reducing the diffusion length of the hydrogen, thus achieving the minimum onset desorption temperature.^{24,51}

To have a better understanding on the reaction process and mechanism of this sample, XRD measurements were performed on $\text{MgH}_2 + 10 \text{ wt.}\% \text{ Co}_2\text{NiO}$ samples after 1 h of milling, after dehydrogenation at 250 °C, after dehydrogenation at 450 °C, and after rehydrogenation at 320 °C under 30.0 atm hydrogen pressure, as shown in Fig. 10. After 1 h of milling, the MgH_2 and Co_2NiO peaks were seen to dominate the XRD pattern with few Mg peaks. Mg peaks

appeared at this stage confirmed there was hydrogen released during ball milling. After heating to 250 °C, it was seen that the same peaks appeared, such as those in ball milling. Further heating to 450 °C caused MgH₂ and Co₂NiO to disappear. The dehydrogenation of MgH₂ can be confirmed with distinct Mg peaks, and the transformation of MgH₂ into Mg can be represented as follows:



MgO peak was also detected in the dehydrogenation spectra due to slight oxygen contamination when transferring the samples to the XRD instrument. In addition, new Mg-Co alloy and Co_{1.29}Ni_{1.71}O₄ peaks could also be seen. The presence of Mg-Co alloy and Co_{1.29}Ni_{1.71}O₄ might have appeared during the dehydrogenation process. XRD examination of the dehydrogenated MgH₂ doped with Co₂NiO sample verified the formation of Mg-Co alloy and Co_{1.29}Ni_{1.71}O₄ peaks and these peaks remained unchanged after rehydrogenation at 320 °C. Hence, we speculate that the Mg-Co alloy and Co_{1.29}Ni_{1.71}O₄ species could have acted as the real catalysts. In addition, it was seen that Mg was largely transformed into MgH₂ after the rehydrogenation process.

In order to investigate the Co₂NiO containing phase after dehydrogenation in detail, we prepared a MgH₂ + 50 wt.% Co₂NiO sample, as it was difficult to analyse the phase composition with 10 wt.% Co₂NiO by XRD. Fig. 11 shows the XRD patterns of MgH₂ doped with 50 wt.% Co₂NiO sample (a) after 1 h ball milling, (b) after dehydrogenation at 250 °C and (c) after dehydrogenation at 450 °C. After increasing the amount of Co₂NiO to 50 wt.%, the Co₂NiO peaks increased compared to as-milled MgH₂ + 10 wt.% Co₂NiO sample as shown in Fig 10 (a). Mg peaks were detected in the XRD spectra indicating that hydrogen was released during ball milling. After heating to temperature 250 °C, the same Mg, MgH₂ and Co₂NiO peaks were seen with few Mg-Co alloy and Co_{1.29}Ni_{1.71}O₄ peaks. The formation of Mg-Co alloy and

$\text{Co}_{1.29}\text{Ni}_{1.71}\text{O}_4$ at 250 °C indicates that these active species were formed during the heating process. Further temperature increment to 450 °C saw the disappearance of MgH_2 and Co_2NiO peaks with more frequent appearance of Mg-Co alloy and $\text{Co}_{1.29}\text{Ni}_{1.71}\text{O}_4$ peaks. As compared to the XRD pattern of $\text{MgH}_2 + 10 \text{ wt.}\% \text{Co}_2\text{NiO}$ sample (Fig. 10), the formation of Mg-Co alloy and $\text{Co}_{1.29}\text{Ni}_{1.71}\text{O}_4$ were more discernible after 50 wt.% Co_2NiO was added.

From the results, we speculate that the formation of Mg-Co alloy and $\text{Co}_{1.29}\text{Ni}_{1.71}\text{O}_4$, which resulted from the reaction of MgH_2 and Co_2NiO during de/hydrogenation process, could play an important role in the enhancement of hydrogen sorption. The formation of Mg-Co alloy in this study is mutual with the findings by Mao et al.³⁸ They suggested that Mg-Co alloy formed in the $\text{MgH}_2\text{-CoCl}_2$ system could act as a catalyst besides MgCl_2 alloy, thus improving the de/hydrogenation of MgH_2 through the additive. It can be speculated that, this additive reduces the barrier of nucleation, and thus hydrogen desorption takes place at a lower driving force and the transition metal helps in facilitating the dissociation of hydrogen molecules and the recombination of hydrogen atom towards the molecular state.¹⁴ In addition, it is believed that the newly formed ball-milled or dehydrogenation product in the complex hydride catalyst system could act as a real catalyst to facilitate the de/rehydrogenation steps.⁵² In this study, Co-Ni oxide species with an altered valance state, $\text{Co}_{1.29}\text{Ni}_{1.71}\text{O}_4$, could have acted as a real catalyst because they could create surface activation and form a large amount of nucleation sites at the surface of the MgH_2 matrix. It is also speculated that these finely dispersed ball-milled products could serve as the active sites for nucleation by shortening the diffusion distance of the reaction ions.⁵²

4. Conclusion

In summary, the hydrogen sorption properties of MgH_2 improved after doping it with 10 wt.% Co_2NiO . $\text{MgH}_2 + 10$ wt.% Co_2NiO composite has a lower onset dehydrogenation temperature of 300 °C, which was decreased to about 117 °C and 70 °C compared to as-received and as-milled MgH_2 , respectively. In terms of dehydrogenation kinetics, $\text{MgH}_2 + 10$ wt.% Co_2NiO sample released about 2.5 wt.% hydrogen in 6 min at 320 °C, while as-milled MgH_2 sample showed no hydrogen release under the same condition. Meanwhile, for absorption kinetics, $\text{MgH}_2 + 10$ wt.% Co_2NiO sample absorbed about 2.5 wt.% hydrogen within 1.7 min at 320 °C, but as-milled MgH_2 sample took about 3.4 min to absorb the same amount of hydrogen. The results from the Kissinger plot showed that the activation energy for hydrogen desorption of MgH_2 was reduced compared to those of as-received and as-milled MgH_2 from 183.0 and 133.0 kJ/mol to 118.0 kJ/mol, respectively, after the addition of 10 wt.% Co_2NiO . It is reasonable to conclude that, in this study, the Co_2NiO additive doped with MgH_2 played a catalytic role through the formation of active species of Mg-Co alloy and $\text{Co}_{1.29}\text{Ni}_{1.71}\text{O}_4$ during the heating process. This newly developed product acted as a real catalyst in improving the hydrogen storage properties of MgH_2 .

Acknowledgement

The authors would like to thank the Universiti Malaysia Terengganu for providing the facilities to carry out this project and the Malaysian Ministry of Education for the research grant under Fundamental Research Grant Scheme (FRGS 59362). N. Juahir and N. S. Mustafa are grateful to the Malaysian Ministry of Education for a MyBrain15 scholarship.

Figure captions

Fig. 1 TPD curves for dehydrogenation of the as-received, as-milled and $\text{MgH}_2 + 10 \text{ wt.}\%$ Co_2NiO composite.

Fig. 2 Isothermal dehydrogenation kinetics of the as-milled and $\text{MgH}_2 + 10 \text{ wt.}\%$ Co_2NiO composite at $320 \text{ }^\circ\text{C}$.

Fig. 3 Isothermal rehydrogenation kinetics of the as-milled and doped $\text{MgH}_2 + 10 \text{ wt.}\%$ Co_2NiO composite at $320 \text{ }^\circ\text{C}$ and under 30.0 atm hydrogen pressure.

Fig. 4 Isothermal rehydrogenation kinetics of the as-milled and doped $\text{MgH}_2 + 10 \text{ wt.}\%$ Co_2NiO composite for the ten cycles.

Fig. 5 Isothermal dehydrogenation kinetics of the as-milled and $\text{MgH}_2 + 10 \text{ wt.}\%$ Co_2NiO composite for the ten cycles.

Fig. 6 Recyclability capacity of the $\text{MgH}_2 + 10 \text{ wt.}\%$ Co_2NiO sample after 60 min absorb/desorb for the ten cycles.

Fig. 7 DSC traces of as-received, as-milled and $\text{MgH}_2 + 10 \text{ wt.}\%$ Co_2NiO at heating rate of $15 \text{ }^\circ\text{C}/\text{min}$.

Fig. 8 DSC traces of (a) as-received, (b) as-milled MgH_2 , (c) $\text{MgH}_2 + 10 \text{ wt.}\%$ Co_2NiO at different heating rates of $15 - 30 \text{ }^\circ\text{C}/\text{min}$ and (d) the Kissinger's analysis for (a) as-received MgH_2 , (b) as-milled MgH_2 , and (c) MgH_2 doped $10 \text{ wt.}\%$ Co_2NiO composites.

Fig. 9 The SEM images of the (a) as-received MgH_2 , (b) as-milled MgH_2 and (c) $\text{MgH}_2 + 10 \text{ wt.}\%$ Co_2NiO .

Fig. 10 XRD patterns of MgH_2 doped $10 \text{ wt.}\%$ Co_2NiO (a) after 1 h ball milling, (b) after dehydrogenation at $250 \text{ }^\circ\text{C}$, (c) after dehydrogenation at $450 \text{ }^\circ\text{C}$ and (d) after rehydrogenation at $320 \text{ }^\circ\text{C}$.

Fig. 11 XRD patterns of MgH_2 doped $50 \text{ wt.}\%$ Co_2NiO (a) after 1 h ball milling, (b) after dehydrogenation at $250 \text{ }^\circ\text{C}$ and (c) after dehydrogenation at $450 \text{ }^\circ\text{C}$.

References

1. S. Satyapal, J. Petrovic, C. Read, G. Thomas and G. Ordaz, *Catal. Today*, 2007, **120**, 246-256.
2. G. Liang, J. Huot, S. Boily, A. Van Neste and R. Schulz, *J. Alloys Compd.*, 1999, **292**, 247-252.
3. I. P. Jain, C. Lal and A. Jain, *Int. J. Hydrogen Energy*, 2010, **35**, 5133-5144.
4. J. Huot, G. Liang, S. Boily, A. Van Neste and R. Schulz, *J. Alloys Compd.*, 1999, **293-295**, 495-500.
5. M. Ismail, *Int. J. Hydrogen Energy*, 2014, **39**, 2567-2574.
6. H. Gasan, O. N. Celik, N. Aydinbeyli and Y. M. Yaman, *Int. J. Hydrogen Energy*, 2012, **37**, 1912-1918.
7. M. Ismail, Y. Zhao, X. B. Yu, J. F. Mao and S. X. Dou, *Int. J. Hydrogen Energy*, 2011, **36**, 9045-9050.
8. S. Kurko, A. Aurora, D. M. Gattia, V. Contini, A. Montone, Ž. Rašković-Lovre and J. G. Novaković, *Int. J. Hydrogen Energy*, 2013, **38**, 12140-12145.
9. M. Ismail, Y. Zhao and S. X. Dou, *Int. J. Hydrogen Energy*, 2013, **38**, 1478-1483.
10. H. Liu, C. Wu, H. Zhou, T. Chen, Y. Liu, X. Wang, Z. Dong, H. Ge, S. Li and M. Yan, *RSC Adv.*, 2015, **5**, 22091-22096.
11. M. Ismail, Y. Zhao, X. B. Yu and S. X. Dou, *RSC Adv.*, 2011, **1**, 408-414.
12. N. S. Mustafa, N. H. Idris and M. Ismail, *Int. J. Hydrogen Energy*, 2015, **40**, 7671-7677.
13. J. L. Bobet, E. Akiba, Y. Nakamura and B. Darriet, *Int. J. Hydrogen Energy*, 2000, **25**, 987-996.
14. A. Ranjbar, Z. P. Guo, X. B. Yu, D. Attard, A. Calka and H. K. Liu, *Int. J. Hydrogen Energy*, 2009, **34**, 7263-7268.
15. J. Charbonnier, P. de Rango, D. Fruchart, S. Miraglia, L. Pontonnier, S. Rivoirard, N. Skryabina and P. Vulliet, *J. Alloys Compd.*, 2004, **383**, 205-208.
16. X. B. Yu, Y. H. Guo, H. Yang, Z. Wu, D. M. Grant and G. S. Walker, *J. Phys. Chem. C*, 2009, **113**, 5324-5328.
17. X. B. Yu, Z. X. Yang, H. K. Liu, D. M. Grant and G. S. Walker, *Int. J. Hydrogen Energy*, 2010, **35**, 6338-6344.

18. M. Baricco, M. W. Rahman, S. Livraghi, A. Castellero, S. Enzo and E. Giamello, *J. Alloys Compd.*, 2012, **536**, Supplement 1, S216-S221.
19. K. S. Jung, E. Y. Lee and K. S. Lee, *J. Alloys Compd.*, 2006, **421**, 179-184.
20. S. Milošević, Ž. Rašković-Lovre, S. Kurko, R. Vujasin, N. Cvjetičanin, L. Matović and J. Grbović Novaković, *Ceram. Int.*, 2013, **39**, 51-56.
21. H. Wang, J. Hu, F. Han, Y. Lu, J. Liu, L. Ouyang and M. Zhu, *J. Alloys Compd.*, 2015, <http://dx.doi.org/10.1016/j.jallcom.2015.01.057>.
22. M. Ismail, Y. Zhao, X. B. Yu and S. X. Dou, *Energy Edu. Sci. Technol. Part A Energy Sci. Res.*, 2012, **30**, 107-122.
23. N. Recham, V. V. Bhat, M. Kandavel, L. Aymard, J. M. Tarascon and A. Rougier, *J. Alloys Compd.*, 2008, **464**, 377-382.
24. N. S. Mustafa and M. Ismail, *Int. J. Hydrogen Energy*, 2014, **39**, 15563-15569.
25. F. A. Halim Yap, N. S. Mustafa and M. Ismail, *RSC Adv.*, 2015, **5**, 9255-9260.
26. M. Ismail, *Energy*, 2015, **79**, 177-182.
27. J. Cui, H. Wang, J. Liu, L. Ouyang, Q. Zhang, D. Sun, X. Yao and M. Zhu, *J. Mater. Chem. A*, 2013, **1**, 5603-5611.
28. A. Ranjbar, M. Ismail, Z. P. Guo, X. B. Yu and H. K. Liu, *Int. J. Hydrogen Energy*, 2010, **35**, 7821-7826.
29. C. Z. Wu, P. Wang, X. Yao, C. Liu, D. M. Chen, G. Q. Lu and H. M. Cheng, *J. Alloys Compd.*, 2006, **420**, 278-282.
30. M. Ismail, N. Juahir and N. S. Mustafa, *J. Phys. Chem. C*, 2014, **118**, 18878-18883.
31. H. Shao, M. Felderhoff and F. Schüth, *Int. J. Hydrogen Energy*, 2011, **36**, 10828-10833.
32. A. R. Yavari, J. F. R. de Castro, G. Vaughan and G. Heunen, *J. Alloys Compd.*, 2003, **353**, 246-251.
33. D. L. Croston, D. M. Grant and G. S. Walker, *J. Alloys Compd.*, 2010, **492**, 251-258.
34. W. Oelerich, T. Klassen and R. Bormann, *J. Alloys Compd.*, 2001, **315**, 237-242.
35. H. Simchi, A. Kaflou and A. Simchi, *Int. J. Hydrogen Energy*, 2009, **34**, 7724-7730.
36. C. X. Shang, M. Bououdina, Y. Song and Z. X. Guo, *Int. J. Hydrogen Energy*, 2004, **29**, 73-80.
37. I. E. Malka, T. Czujko and J. Bystrzycki, *Int. J. Hydrogen Energy*, 2010, **35**, 1706-1712.

38. J. Mao, Z. Guo, X. Yu, H. Liu, Z. Wu and J. Ni, *Int. J. Hydrogen Energy*, 2010, **35**, 4569-4575.
39. M. W. Rahman, A. Castellero, S. Enzo, S. Livraghi, E. Giamello and M. Baricco, *J. Alloys Compd.*, 2011, **509**, Supplement 1, S438-S443.
40. O. Friedrichs, J. C. Sanchez-Lopez, C. Lopez-Cartes, T. Klassen, R. Bormann and A. Fernandez, *J. Phys. Chem. B*, 2006, **110**, 7845-7850.
41. S. Kwon, D. Mumm, H. Park and M. Song, *J. Mater. Science*, 2010, **45**, 5164-5170.
42. S. S. Srinivasan, M. U. Niemann, J. R. Hattrick-Simpers, K. McGrath, P. C. Sharma, D. Y. Goswami and E. K. Stefanakos, *Int. J. Hydrogen Energy*, 2010, **35**, 9646-9652.
43. M. Cabo, S. Garroni, E. Pellicer, C. Milanese, A. Girella, A. Marini, E. Rossinyol, S. Suriñach and M. D. Baró, *Int. J. Hydrogen Energy*, 2011, **36**, 5400-5410.
44. T. Mandzhukova, M. Khrussanova, E. Grigorova, P. Stefanov, M. Khristov and P. Peshev, *J. Alloys Compd.*, 2008, **457**, 472-476.
45. T. Mandzhukova, J.-L. Bobet, M. Khrussanova and P. Peshev, *Mater. Res. Bull.*, 2009, **44**, 1968-1972.
46. M. Ismail, Y. Zhao, X. B. Yu and S. X. Dou, *Int. J. Hydrogen Energy*, 2010, **35**, 2361-2367.
47. M. Ismail, Y. Zhao, X. B. Yu, A. Ranjbar and S. X. Dou, *Int. J. Hydrogen Energy*, 2011, **36**, 3593-3599.
48. M. Ismail, Y. Zhao, X. B. Yu, I. P. Nevirkovets and S. X. Dou, *Int. J. Hydrogen Energy*, 2011, **36**, 8327-8334.
49. M. Ismail, A. Sinin, C. Sheng and W. W. Nik, *Int. J. Electrochem. Sci.*, 2014, **9**, 4959-4973.
50. H. E. Kissinger, *Anal. Chem.*, 1957, **29**, 1702-1706.
51. H. Gasan, N. Aydinbeyli, O. N. Celik and Y. M. Yaman, *J. Alloys Compd.*, 2009, **487**, 724-729.
52. F. Zhai, P. Li, A. Sun, S. Wu, Q. Wan, W. Zhang, Y. Li, L. Cui and X. Qu, *J. Phys. Chem. C*, 2012, **116**, 11939-11945.

Figures

Figure 1

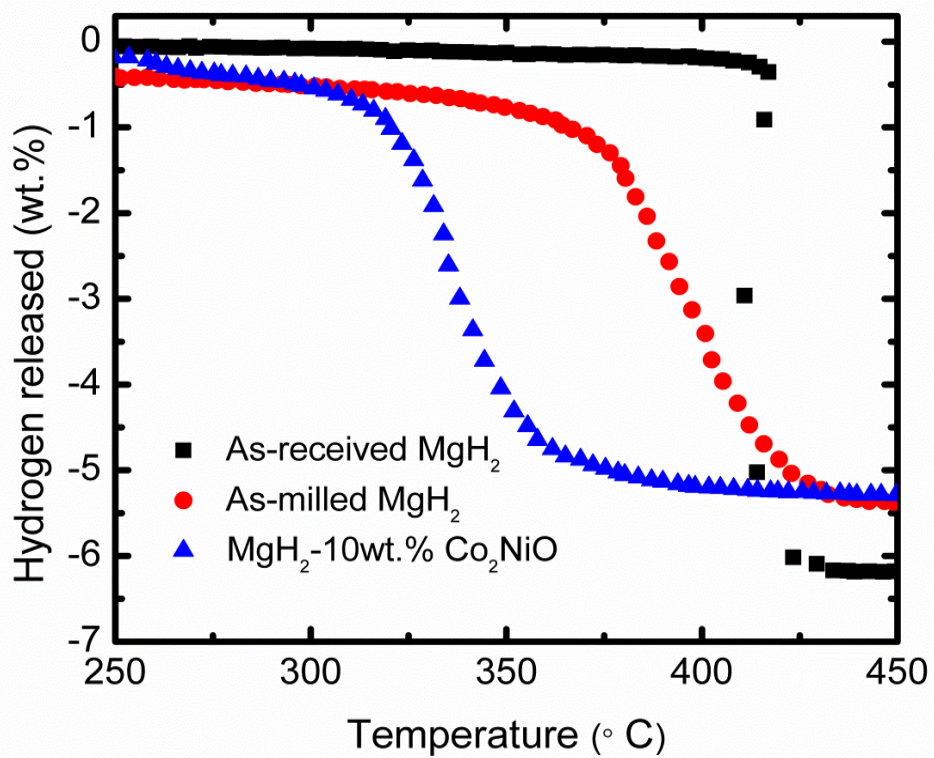


Figure 2

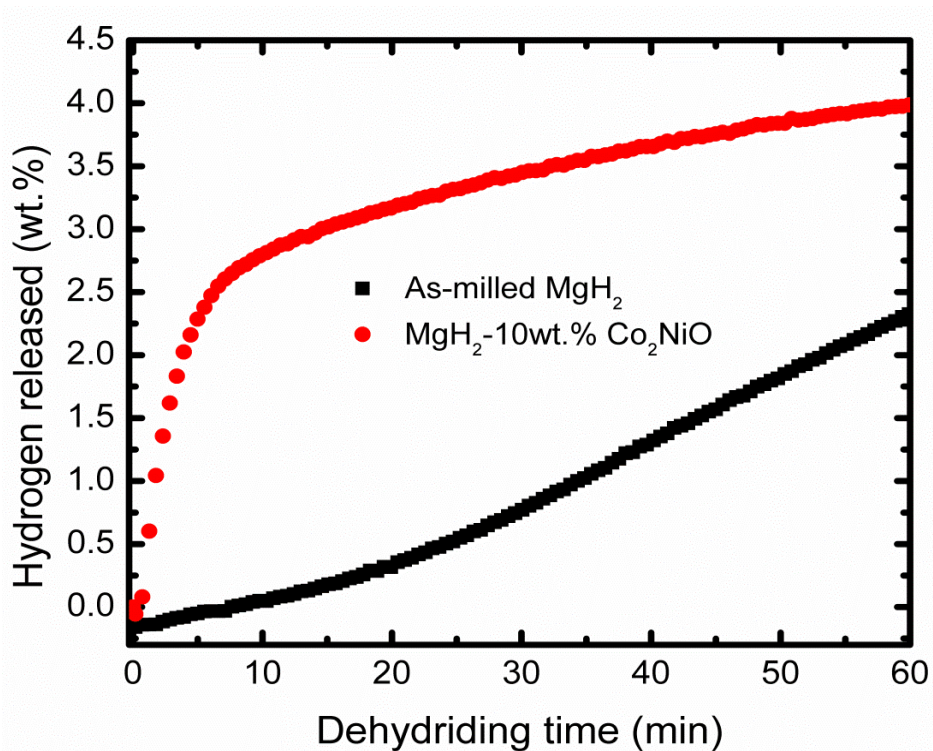


Figure 3

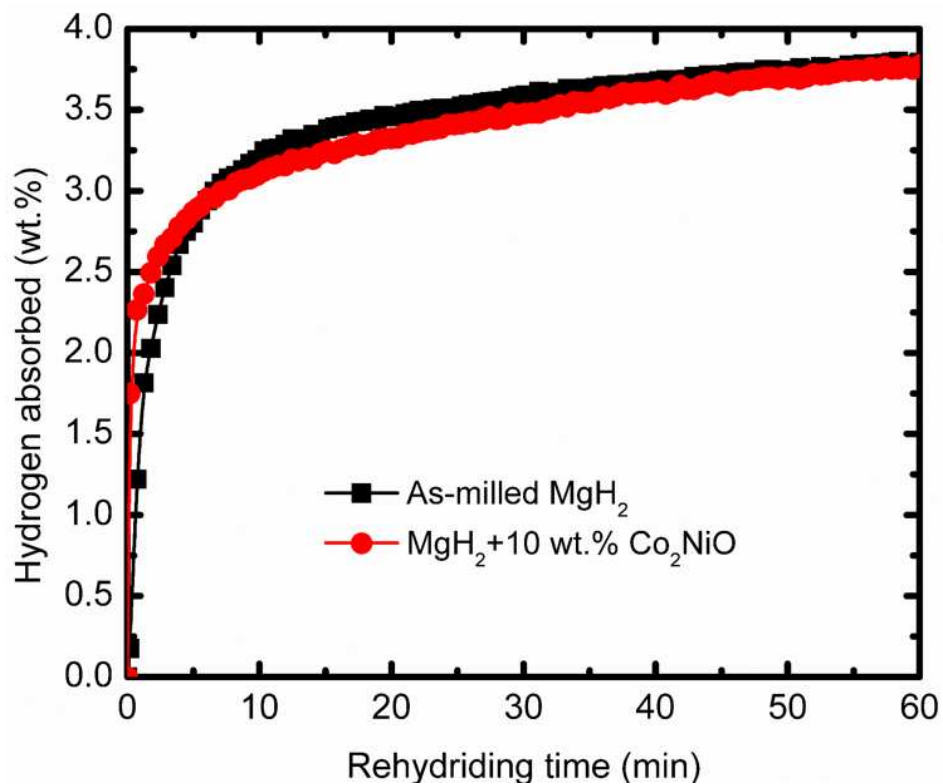


Figure 4

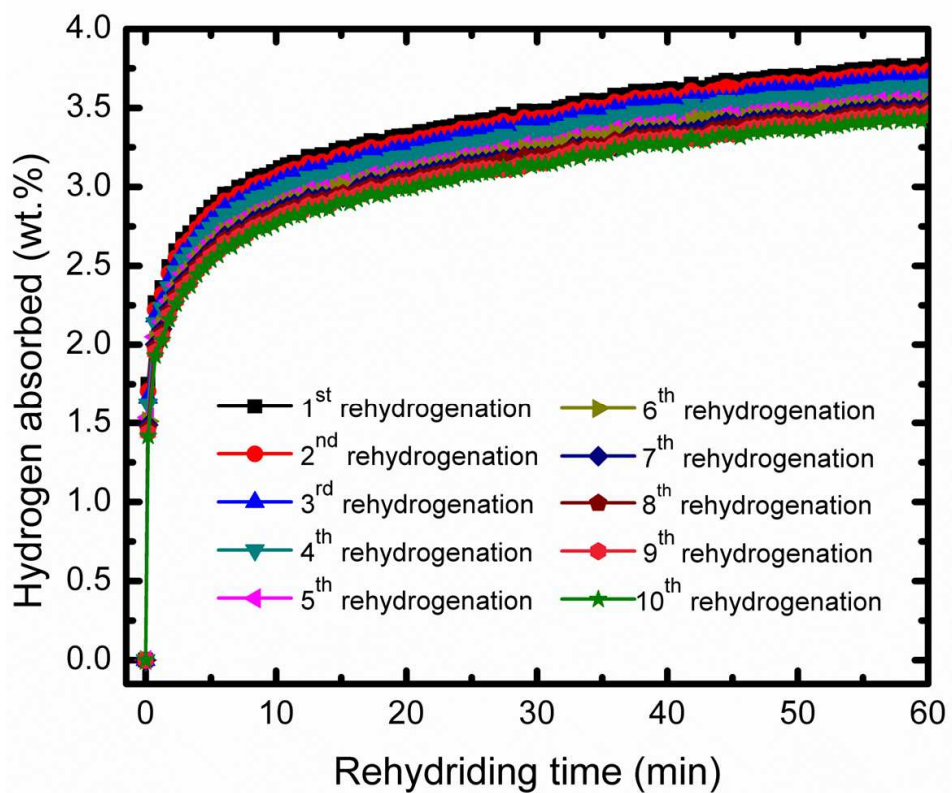


Figure 5

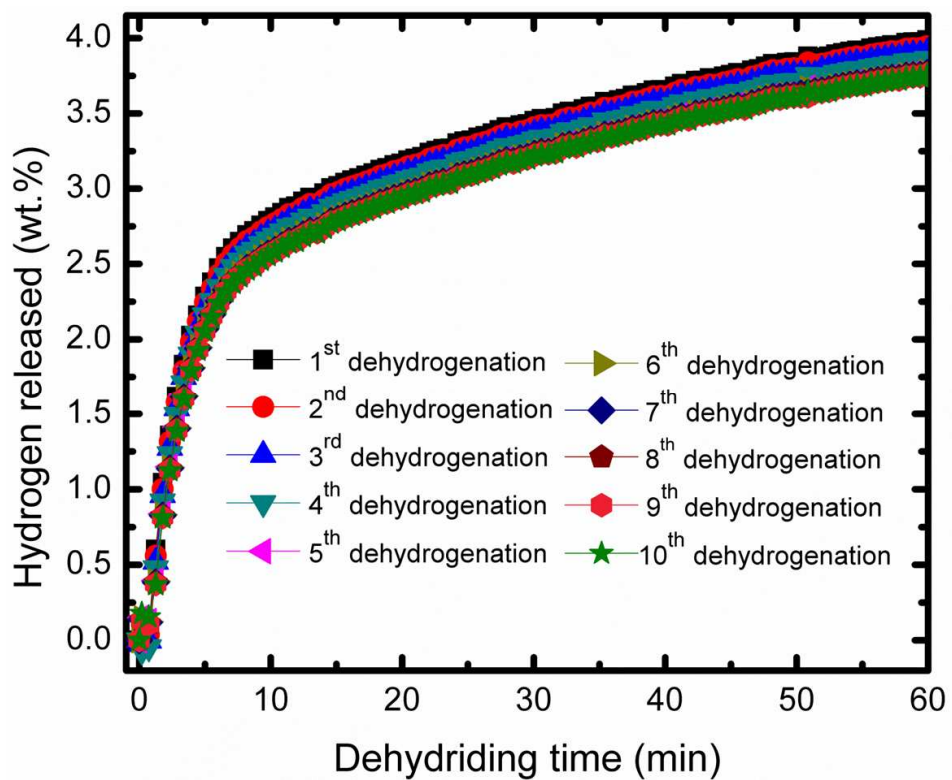


Figure 6

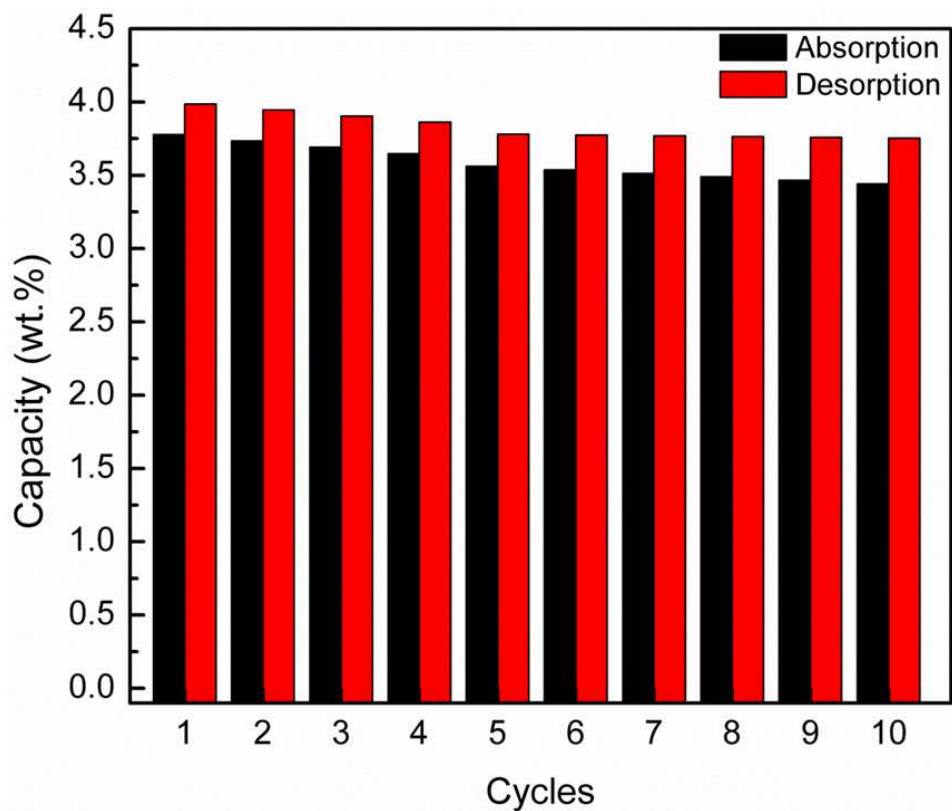


Figure 7

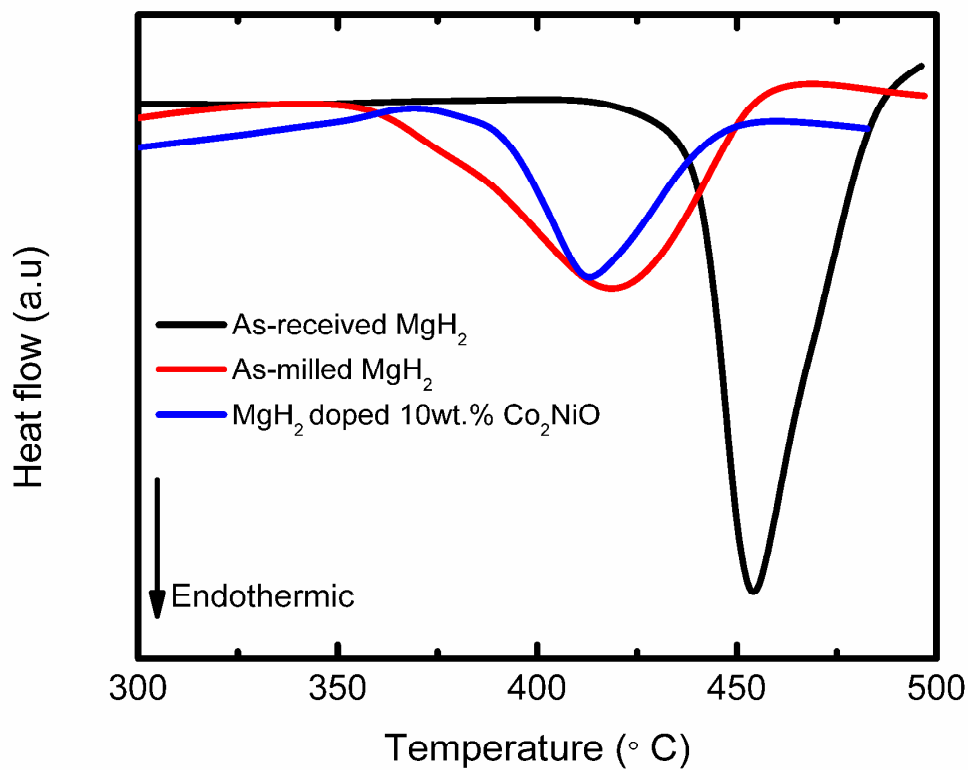


Figure 8

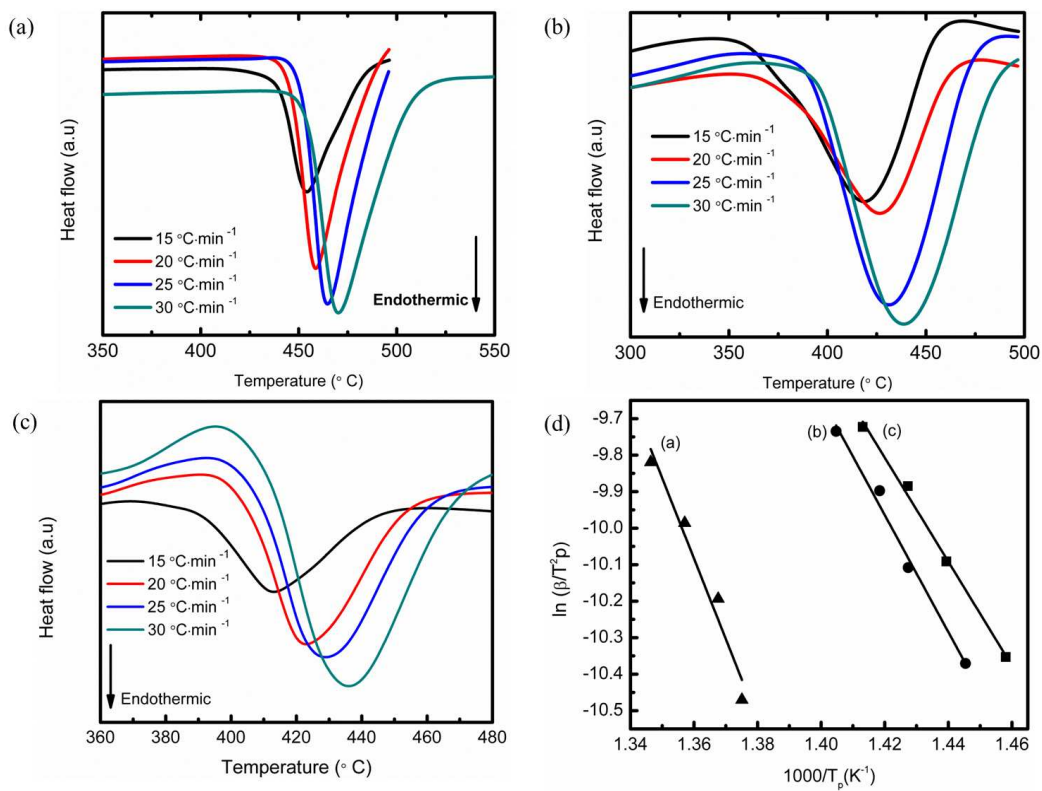


Figure 9

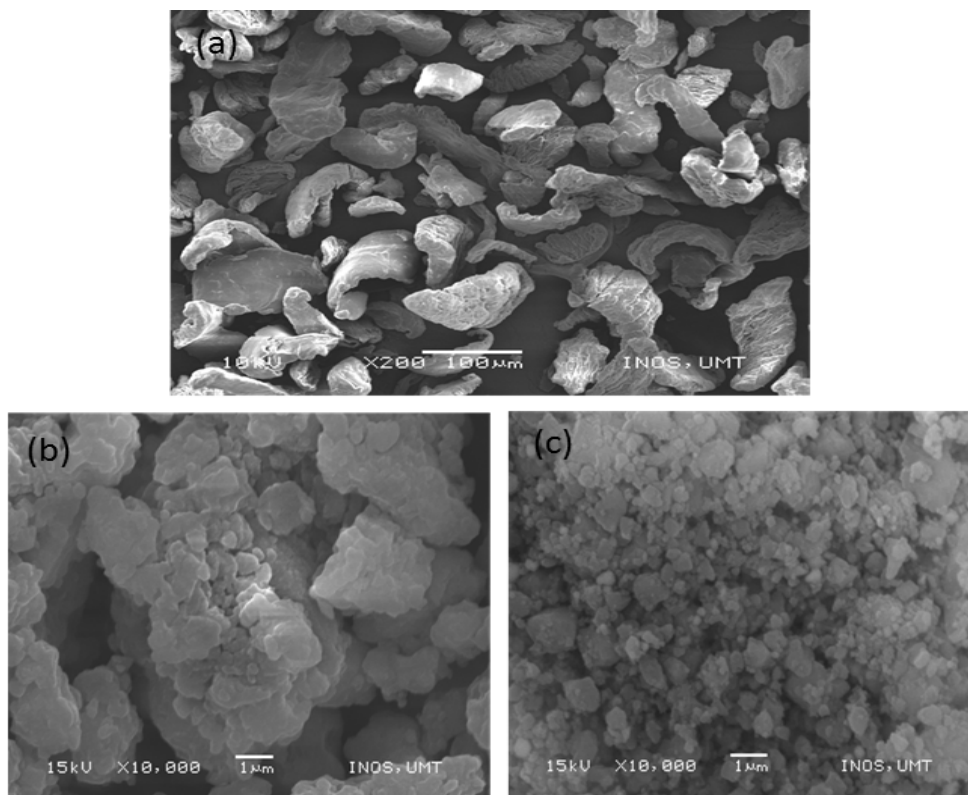


Figure 10

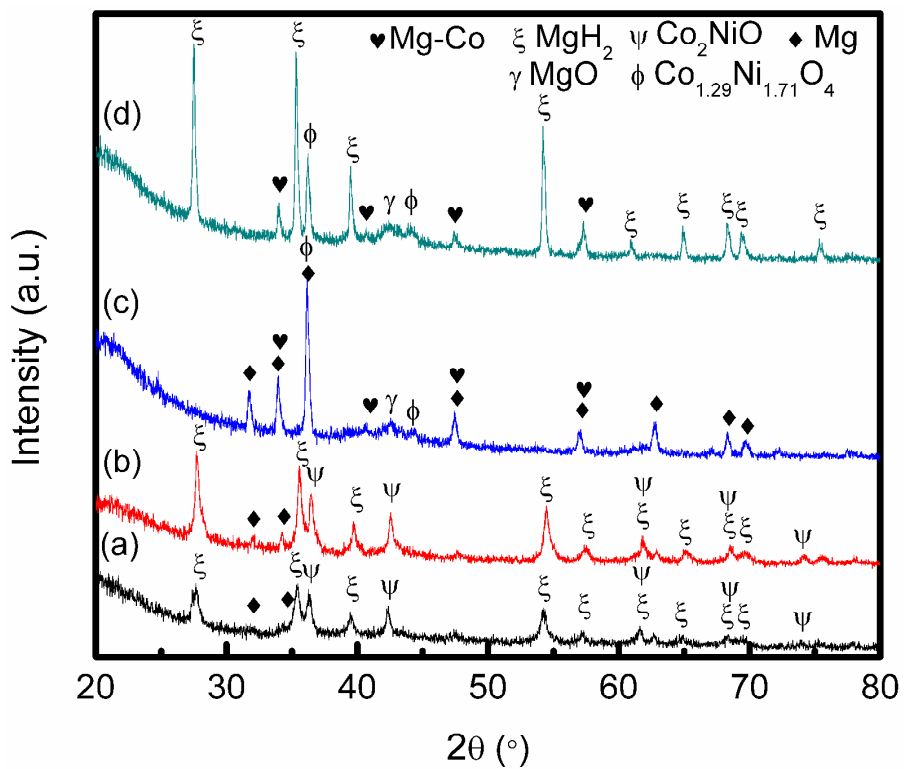


Figure 11

